Documentation of the Gaia Ecliptic Pole Catalogue (GEPC)

prepared by: M. Altmann
approved by:
reference: GAIA-C3-TN-ARI-MA-015-1
issue: 1
revision: 0
date: 2013-12-18
status: Issued

Abstract

The GEPC3.0 is the third major release of the Gaia Ecliptic Pole Catalogue encompassing the GEPC2.1 and the full $ugriz$ photometry as well as two epoch astrometry for the Northern ecliptic pole field (NEP). The GEPC2.1 (these data are unchanged in the present version) is the second major release of the Gaia Ecliptic Pole Catalogue encompassing all of the 1 epoch photometric and astrometric data (U-band data coming from another source will be added later). It contains $UBVI$ photometry for the complete Southern EP-field, and the according G-magnitudes ($G, G_{RVS}, G_{BP}, G_{RP}$) as well as precise positions.

Contents

1 Introduction

The "Gaia Ecliptic Poles Catalogue" (GEPC, formerly known as "Ecliptic Poles Catalogue", EPC) was conceived to serve as reference fields for the commissioning phase which will be frequently visited by Gaia's telescopes. During the Gaia commissioning phase the spacecraft will operate on a scan law different from the nominal one, namely the "Ecliptic Poles Scan Law" (EPSL), see BV-001. This scan law implies that both apertures will scan the Ecliptic Poles (EP) on every rotation of the space craft, slowly preceding around each EP. This makes the fields around the EP's the natural test fields. The specifications of the GEPC are described in detail in BV-001 and also in MA-002. It has since been decided to incorporate the GEPC into the "Initial Gaia Source List" (IGSL), see RLS-004, which also includes all known stars outside of the EP-fields. The objects in the IGSL which are in the EP-fields covered by the GEPC, are marked with a flag in the IGSL. For more details about the IGSL, please refer to the IGSL documentation (RLS-004)[1]. The version of the GEPC included in the IGSL is the current version GEPC3.0.

1.1 Characterisation of the two fields

The fields around the Ecliptic Poles are located at moderate Galactic latitudes and longitude-wise almost orthogonal to the line Galactic Centre - Anticentre. (see Table 1). Hence they in principle have comparable densities of Galactic stars. However the southern field lies in the outskirts of the Large Magellanic Cloud (LMC), which adds the bulk to the stellar contents of the catalogue, especially at fainter magnitudes, where LMC stars are the dominant population.

TABLE 1: Celestial and Galactic coordinates of both fields. It was aimed to centre the catalogue on these coordinates, however pointing inaccuracies etc. will have produced a small shift of several arcseconds. The column "#stars" gives the number of stars for each field in the catalogue

Field	α_{2000}	δ_{2000}	l^{II}	b^{II}	#stars
NEP	18:00:00	+66:33:41	96.3840	+29.8114	164468
SEP	06:00:00	−66:33:41	276.3840	−29.8114	448478
GEPC	—	—	—	—	612946

TABLE 2: List of proposals delivering data for this programme

Date	Observatory	Tel.	Instr.	Obs.Type	Proposal ID	P.I.	Observer	Field	Summary
Nov./Dec. 2007	ESO-LaSilla	MPI2.2m	WFI	Imaging	080A.9001	K. Meisenheimer	K.Meisenheimer	S	VR_c data secured for 4/5 of the field, SW pointing missing - no calibration data
Jan. 2009	ESO-LaSilla	MPI2.2m	WFI	Imaging	082A.9018	K. Meisenheimer	M. Altmann	S	Full set of BVR_cI_c data secured, calibration
Jul. 2009	Mauna Kea	CFHT 3.6m	MEGACAM	Imaging	2008AO02	M. Altmann	Queue	N	$ugri$ photometry/astrometry for NEP field
Jan. 2010	NOAO-CTIO	4m-Blanco	MOSAIC2	Imaging	2009B-0166	M.Altmann	M. Altmann	S	U-band photometric data
Jul. 2011	Mauna Kea	CFHT 3.6m	MEGACAM	Imaging	2008AO02	M. Altmann	Queue	N	ri imaging of NEP for astrometry
Jan. 2012	ESO-LaSilla	MPI2.2m	WFI	Imaging	086A.9005	K. Meisenheimer	K.Meisenheimer	S	2nd epoch R_cI_c data secured for astrometry

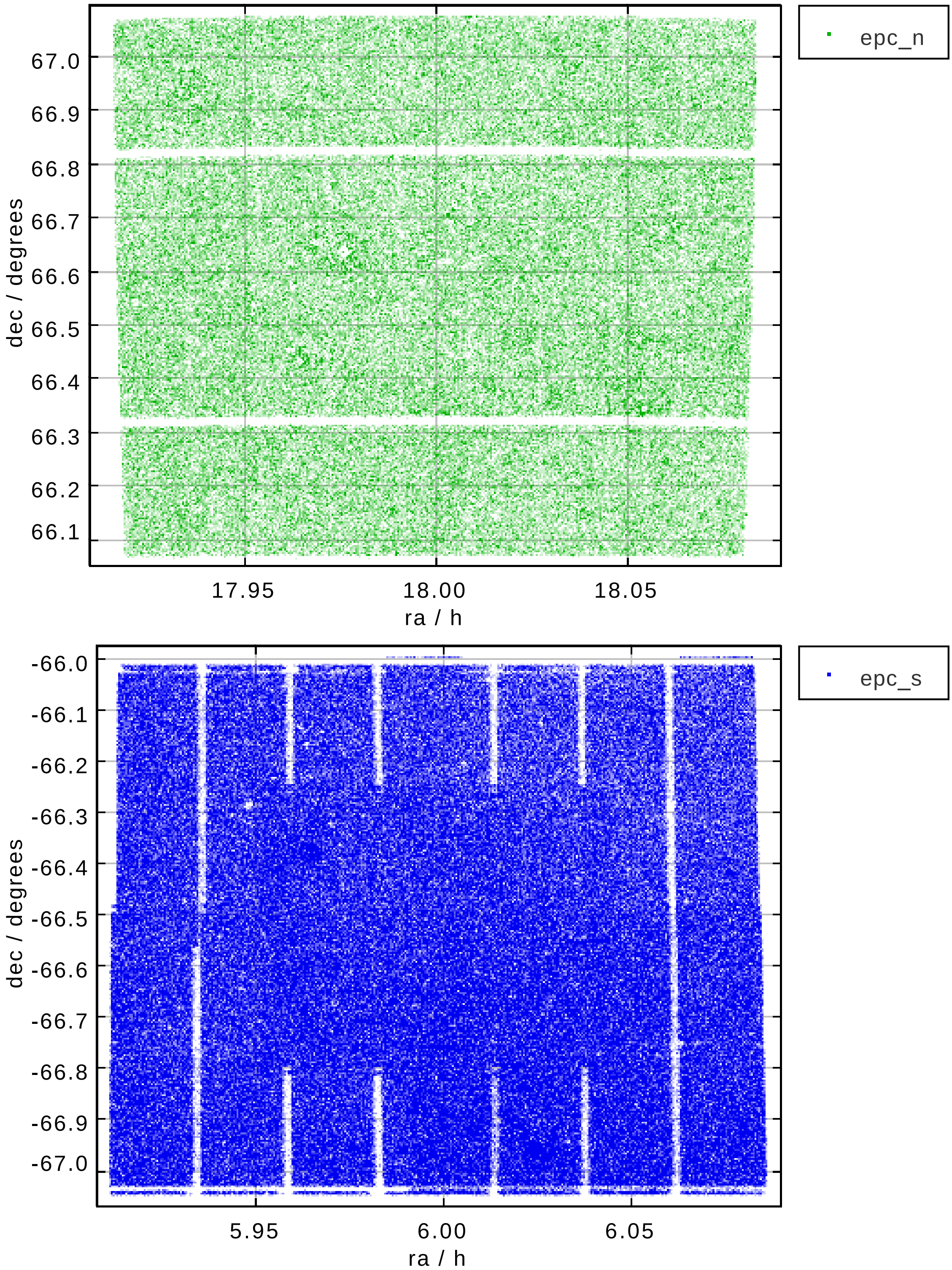

FIGURE 1: The coverage of the GEPS fields. The upper panel shows the northern the lower one the southern field. The gaps or underpopulated regions are caused by the dither pattern, the conical shape is due to the high declination, so that the $\sin \delta$ factor already has a significant influence on the 1 degree level. In reality the fields are more or less square.

2 The Data

2.1 The Northern Field

The data was taken with the CFHT 3.58 m telescope located on Mauna Kea (Hawaii) and its MEGACAM detector. This instrument features 36 2Kx4K pixel chips arranged in a 9x4 chip matrix and has a FOV of approximately 1x1 degrees. Pixel scale is 0.188”/pix, i.e. somewhat better than the 0.238”/pix of WFI and the 0.27”/pix of MOSAIC2 of the 4 m Blanco telescope on Cerro Tololo (Chile). The larger FOV means that 1 pointing is sufficient to cover the whole field. On the downside, the 4 row arrangement of the individual detectors results in gaps in the field, if one uses an efficient dither pattern, i.e. one that does not lead to too much readout and repositioning overhead caused by too many sub-pointings (re-pointings during execution of dither pattern). We have chosen a standard 5 sub-pointings dither pattern, similar to the one used in the south with WFI. The data used for this release was taken in service mode during summer 2008 and 2010. An earlier epoch, dating from 2004 (obtained by Hwang et al.), was retrieved from the CFHT. Due to problems with the astrometric reduction of this data (which has images from two detectors half missing, because of defect amplifiers), this data is not included in this release. This may happen at a later stage, when/if these problems are solved. However we do include the z-photometry from (Hwang et al., 2007) , since we did not obtain z-band data; we also use their catalogue to calibrate our photometry. The astrometry of Hwang et al is severely compromised, with systematic residuals of up to more than 1 arcsec.

2.2 The Southern Field

The current release contains all of the $BVRI$ data taken in two observing runs in November 2007 and January 2009 using the WFI detector mounted on the 2.2m MPIA telescope at La Silla in Chile. Unlike in version one both deep and shallow data are used. The shallow exposures have an exposure time of 10 sec in each passband, the deep ones 160 sec for I and V, 120 sec for R and 190 sec for B-band. In order to cover the gaps in the mosaic a standard 5 exposure dither pattern has been used, and to fill the complete field of 1 square degrees 5 different pointings were used, one in the centre, four shifted by about 14’ both in RA and DEC. In 2007 only R and I data for four fields could be acquired, with one corner missing. This has been rectified in a second run 2009, and two more passbands were added.

For the southern field, U-band data was secured in January 2010 using the 4 m Blanco telescope at Cerro Tololo Interamerican Observatory (CTIO) in January 2010. This data, which is not required for the commissioning phase of Gaia, will be added to the catalogue in version 4.0.

[1]Please note, that stars brighter than 12th or 13th mag are not in the current version of the GEPC, they are however also marked in the IGSL

2.3 Cautionary notes about Mosaic data

This section is especially intended for readers not familiar with Mosaic-type detector arrays or astronomical CCD detectors on the whole. All others may skip this part.

The spatial CCD data for both fields have been obtained with so-called Mosaic-type detectors[2], usually the only way to cover a field of a size near in the order of 1 square degrees in an effective way. A Mosaic-type detector consists of a number of tiled CCD detectors rather than one monolithic CCD chip. The number of individual CCDs can range from two to almost infinite. The reason this is done is that monolithic CCDs of the size required are either too expensive, have physical problems or simply do not exist[3].

The user of this data, or in fact any data of this kind should be aware that this mosaicing comes at a price. While care is taken, that the impact of adverse effects are minimised, there will still be residual effects in terms of PSF-size and -shape (which is determined by the ambient seeing, the optics, the focus which will vary from chip to chip since they are not exactly in the same plane (and tilted - which is also true for single detectors), etc.), the depth, background and saturation. Since the individual chips do not fit gapless to each other, each exposure will have gaps in the sky coverage. This is usually mitigated by using dither patterns, the cost of which is that the depth variation is even larger. Dithering also mitigates the adverse effects of bad columns, which are not uncommon in these kind of detectors. In more complicated setups, such as the 4×9 chip CFHT-Megacam device, used for creating the northern part of this catalogue, reasonably simple dither patterns will not close the gaps completely, see Fig. 1, upper panel.

2.4 Instrumentation and general characterisation of the data

The data used for the GEPC come from two different detector systems[4] with different characteristics, and thus advantages and disadvantages.

The northern field was observed with the $4{\times}9 \times 4K \times 2K$ MEGACAM array located on the 3.57 m CFHT on Mauna Kea, Hawaii. This device allows the full coverage of 1×1 degrees in one exposure, however given the 4 rows of CCD chips together with gaps of different breadths, they cannot be closed completely with a 5 exposure dither pattern. On the other side since the whole field is covered with each shot, the seeing, background and depth will be uniform over the entire field, apart from those parts covered by gaps during the dithering. The other effects influencing the PSF will however also prevail in this data.

[2]Gaia itself also has a Mosaic-type detector with 106 CCDs

[3]Currently the largest CCD-Chips are 8-9.5 cm×8-9.5 cm, such as the one of the Lowell Observatory Large Monolithic Imager (LMI), see http://www.lowell.edu/news/2012/09/lowells-nsf-funded-large-monolithic-imager-sees-first-light-on-the-discovery-channel-telescope/. A significantly larger size will be unrealistic given the typical Si-Wafer size

[4]Eventually it will be three systems, adding the CTIO-Mosaic2 detector for the U-band data of the southern field. However its characteristics are in principle very similar to those of the MPIA-ESO2.2m-WFI setup

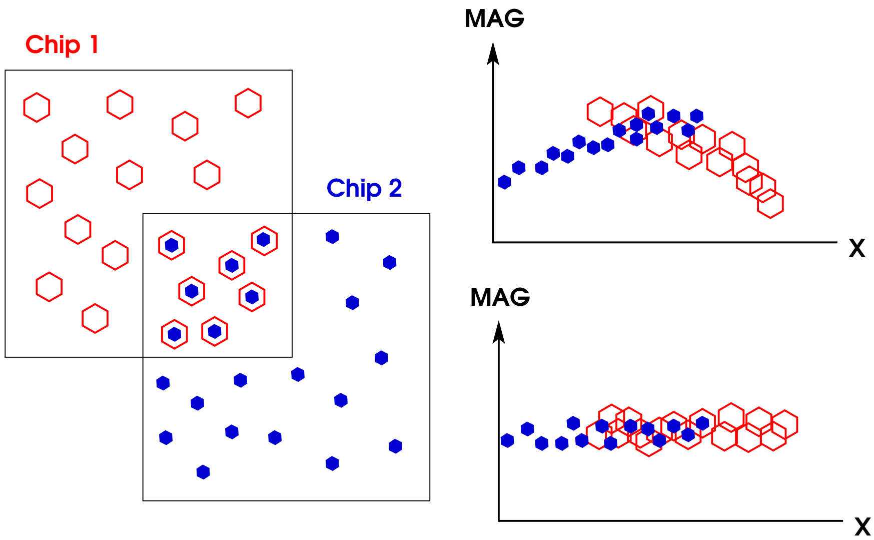

FIGURE 2: Schematic view of how overlapping fields could reveal photometric field gradients. On the left the geometric situation of two pointings with an overlap of 1/4 of the field including the centre is shown. The red and blue hexagons are the stars depicted on each exposure, those where the symbols overlap are the ones common to both exposures. The stars shown here are all assumed to be of the same brightness. The graphs on the right hand side show a strong gradient towards e.g the centre, like those caused by vignetting and improper (too weak) flat fielding (above) and the ideal situation (below), where both magnitudes overlap, apart from the stochastic scatter. In the southern field of this catalogue (the northern doesn't have overlaps, see text) the situation is like the lower plot as it should be.

The southern field was observed with a $2\times4\times4K\times2K$ array (WFI mounted to the MPIA/ESO2.2m at La Silla observatory), which only covers 0.5×0.5 degrees. Therefore apart from the dithering to close the detector gaps a larger pointing pattern of at least 4 pointings is required to cover the full field. We have chosen a 5 pointing pattern, with one pointing in the centre and the other four centred half way out from the centre covering each corner. This means that due to varying ambient conditions of the exposures (which are up to more than one year apart) the seeing, transparency, sky background, etc. are different. Our pointing pattern has the property, that the central part of the field is deeper than the outer part. An advantage of this setup is also that vastly different parts of the detector overlap in some parts of certain exposures, allowing to detect any unwanted gradients in the photometry, which could caused by field concentration, vignetting, improper flatfielding or other effects of wide field imagers. These would show up in these overlapping parts as systematically offset values to the rest in some parts while not in others (see Fig. 2).

2.5 Data reduction

2.5.1 Northern field

The northern field was delivered with the basic detrending (de-biassing, flatfielding, etc.) done by the Elixir-pipeline (see e.g. Magnier & Cuillandre (2004)). Further steps including the source extraction was conducted with the Theli program (Schirmer, 2013), available under `http://www.astro.uni-bonn.de/theli/`, based on the Astromatix Suite (Bertin et al., 2012), see also `http://www.astromatic.net/`, which includes well-known programs such as Sextractor (Bertin & Arnouts, 1996). The final assembly and matching of the extracted catalogues including the calibration to Hwang et al. (2007) was done using TOPCAT, a VO-compatible table calculation and plotting tool[5] or the underlying stilts routines, see Taylor (2005), or `http://www.star.bris.ac.uk/~mbt/topcat/` resp. `http://www.star.bris.ac.uk/~mbt/stilts/`. Since Theli delivers flux conserving images, the source extraction was done using the sky projected images, with the centre being the nominal coordinates of the NEP-field. This means that in contrast to the southern part, the source coordinates were already in one common plane/projection and did not need to be transformed further.

2.5.2 Southern field

The WFI-data, see Table 2 was delivered as raw data including calibration data, and had to be reduced from scratch. Calibration data used, are the usual sets of bias and twilight flat data, as well as sky flats derived from the longer exposed science data. Additionally so called ”beta”-images were used to save some of the unfortunately rather frequent ’bad columns”. These images were images exposed to different exposures of β-radiation which allow the correction

[5] Most plots in this document were also made with TOPCAT

of some of the bad columns, namely those which do show a signal response (opposed to those which don't, i.e. dark or hot dead columns). Nonetheless this did not completely work in every case, so some residual columns remain, which leads to the detection of spurious objects along these columns. As a consequence we decided to use harsher rejection methods in the matching process, eliminating the vast majority of such objects, at the cost of missing some others. For the Gaia commissioning, the catalogue is optimised for as few false positives as possible. The reduction of the SEP-data was done using MPIAphot (Meisenheimer, Roeser, priv comm.) a Midas based routine suite developed at the MPIA mainly for reduction of MPIA instruments, such as those on Calar Alto and the 2.2 m MPI-telescope on ESO's La Silla observatory, including the WFI detector used here. The photometry was derived from the non sky projected images (The sky projected images made with MPIAphot are not flux conserving), sources were again extracted with Sextractor (Bertin & Arnouts, 1996). The extracted sources were then brought into one gnomonic plane centred on the centre of the first image of the central pointing using Midas routines.

2.5.3 Stacking and matching

The stacking and matching of individual images was done in a similar fashion for both fields; Therefore this step is described in one part. This process was not done using the actual images, but the extracted sources, see previous Sections. After matching and before combining the data, photometric offsets were determined, and an r.m.s. error was derived. One image (usually the first in the sequence) was chosen to be the reference image, and the others were corrected for the offset to match the reference. Then the stacking of the images was done the following order and the standard deviations of magnitudes and gnomonic coordinates Ξ, η were derived for error determination, see Sect. 3.1 and equation 1). The optimum matching radius was determined to be 0.6" for both fields[6]. For the next steps after the first match (where applicable) the errors were calculated by error propagation:

1. all images of one exposure time and one passband (and one pointing in the case of the south).
2. all results from step 1 for all pointings (only for the south, since the north only has one pointing)
3. all results from step 1 (north) or step 2(south) from one passband
4. all passbands were matched (not stacked, of course)

Finally the photometry was calibrated and the plane of the combined images was transformed to spherical celestial coordinates via gnomonic projection. Calibration and astrometry are described in more detail in Sections 3 and 4

[6] This is not surprising since the average seeing was 1" in both cases

TABLE 3: Arrangement of the various passbands in the catalogue. The photometric systems used to construct this catalogue come from two different photometric systems (see text). Care has been taken to match them so that the most similar ones coincide. Note, the I/i and U/u bands are very similar in both systems.

SEP	NEP	Remarks
U	u	SEP: available with EPC4.0
B	–	
V	g	
R	r	
I	i	
–	z	err_z empty

2.6 Spectroscopic data

This section will be filled in once the spectroscopic data is available and part of this documentation.

3 Photometry

GENERAL NOTE: Both regions use different filter systems, the South, Johnson-Cousins-Bessel (JCB), and the North Sloan filters. These are similar but have distinct differences. Sloan does not have a B-band and JCB does not have z. The Sloan g band is actually roughly speaking a combined $B + V$ JCB filter. The U/u and I/i passbands are similar in both systems, actually the U-band in the south is also Sloan (the U-Band for the SEP-field will be available in EPC4.0). Therefore the photometry columns are arranged in the following way:

so that the most compatible bands are grouped together. For the final version of the GEPC, which will include other photometry (Hipparcos, photographic, etc.) flags will be introduced to denote the relevant filter system.

NORTH: With the photometry from (Hwang et al., 2007) available, which comes from the same instrumentation as our data, we calibrated our photometry to that of (Hwang et al., 2007). In the case of the z band, for which we did not obtain own data, we adopted their values. Since they do not give errors, the error column is nilled in the GEPC3.0.

The conversion to G-magnitudes was done using the g,r-bands and the latest version of the conversion functions by CJ-041.

SOUTH: This release contains four colour BVRI photometry calibrated to the Landolt secondary standard system. The filters used are Johnson-Cousins resp. Bessel filters, available for

TABLE 4: List of used filters and their characteristics. "CWL" stands for "*C*entral *W*ave*L*ength, PWL for "*P*eak *W*ave*L*ength

Filter name	CWL Å	FWHM Å	PWL Å	Peak Transmission %
$BB\#B123\_ESO878$	4511	1335	5025	88.5
$V/89\_ESO843$	5395.62	893.86	5230	87.0
$R/162\_ESO844$	6517.25	1621.84	6685	93.9
$BB\#I203\_ESO879$	8269	2030	7600	87.0
u^*	3740	740		69.7
g'	4870	1450		84.6
r'	6250	1210		81.4
i'	7700	1450		89.2
z'	n/a	n/a		90.2

the WFI instrument.

Since all filters deviate a little from the original, and filter throughput are changed in time by oxidation and other degrading effects, there will always be small residual systematic effects, most of which can be dealt with during calibration, some however will remain.

For this release, individual photometric errors have been derived. These reflect the internal errors only, there are more uncertainties introduced by calibration and various effects, such as filter degradation and others. The true photometric error will thus be larger than the errors listed.

Because of the lack of suited calibration data in the dataset on which the GEPC 1.x was based on, it only has a rough photometric calibration based on the position of the LMC Red Clump. This has been changed in this version, the photometry is now calibrated to the Landolt secondary standards (for more details see Appendix 1). The standard field used for the photometric calibration were T PHE, PG0231+051, SA95-42, and RU 149. The magnitudes are of Vega type (rather than AB). For the northern part, the SDSS type magnitudes are AB by definition.

Important Note: This means that the photometric calibration of the Northern and Southern part are different, the SEP-field is calibrated into the Vega-system, the NEP-field into the AB-system. While this allows straightforward transformation into G-magnitudes (see CJ-041) one can not and must not use the measured magnitudes listed in the GEPC for both fields combined without correction of one system in to the other - you would be making errors of up to 1 mag[7]! By design the derived magnitudes ($G, G_{\mathrm{BP}}, G_{\mathrm{RP}}, G_{\mathrm{RVS}}$) are in the same system, allowing for some systematic small offsets for more out of the ordinary

[7] apart from some of the filters having significantly different characteristics in the south than in the north, especially the V and G_{SDSS} bands

stars[8]

The Conversion to Gaia G magnitudes was done using a different relation also taken from CJ-041. The reason for this is that the I band is the shallowest data, so moving to the $V - R$ vs G instead of the $R - I$ vs G relation will yield G magnitudes for significantly more stars. Since that document is frequently updated, the G-magnitudes will be updated to the newest relations in every new version as well.

3.1 Errors

The magnitude errors are computed by deriving the scatter and then the errors of the single values for each star. The according standard equation is:

$$dMag = \sqrt{\frac{1}{n}} \cdot \sigma_{Mag} = \sqrt{\frac{1}{n(n-1)}} \sqrt{\sum_{i=1}^{n} (\overline{Mag} - Mag_i)} \qquad (1)$$

with n being the number of detections and σ_{Mag} the standard deviation. When combining data of different exposure equation 1 was carried out for every set separately and the error of the combined data was derived by error propagation.

A note of caution: Stars with only one or two detections will have an error of zero, or a quite unrealistic one. Some (a few) objects have a r.m.s. error much larger than others of comparable magnitude. In most cases this hints at variability, taking into account that most of the data were not observed on the same day, and in some cases a year lie between different parts of a dither series, etc.

The photometry errors given in the catalogue are internal r.m.s. errors only. They do not include other systematic sources of error, such as calibration errors, photometry errors of non-point sources, brightness/colour related errors, etc. At least in the southern field, zonal errors, which may be caused by non-prefect flat fielding are partly taken into account due to the 5 point pointing pattern (the dithers in both fields are not offset far enough to show the effects, see Sect. 2.3). As a conservative assumption a systematic accuracy of 0.1 mag is mandated.

4 Astrometry

The astrometry was improved, so that systematic astrometric inaccuracies, as present in GEPC 1.x have been corrected. Analysis shows no detectable mid frequency systematics to our pre-

[8] taking into account that no single polynomial or other relation can account for all spectral features of all species of objects

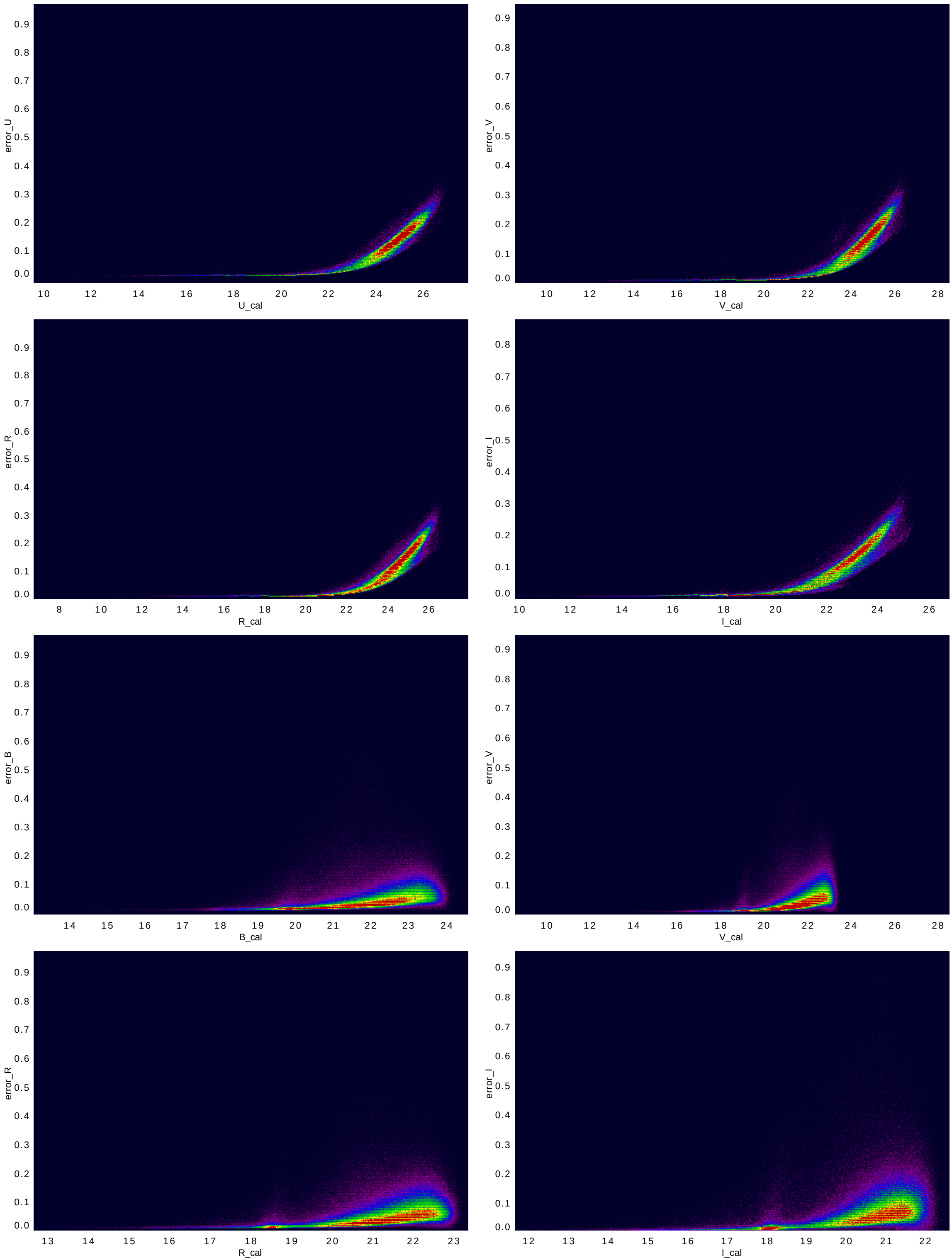

FIGURE 3: The r.m.s. errors of the GEPC photometry. The upper four panels show the situation for the northern field in the sequence u, g, r, i (upper left to lower right), the lower panels show the southern part in the sequence B, V, R, I (upper left to lower right). Please note that these plots represent the internal error only, external errors due to calibration, photometric system, etc. are not included.

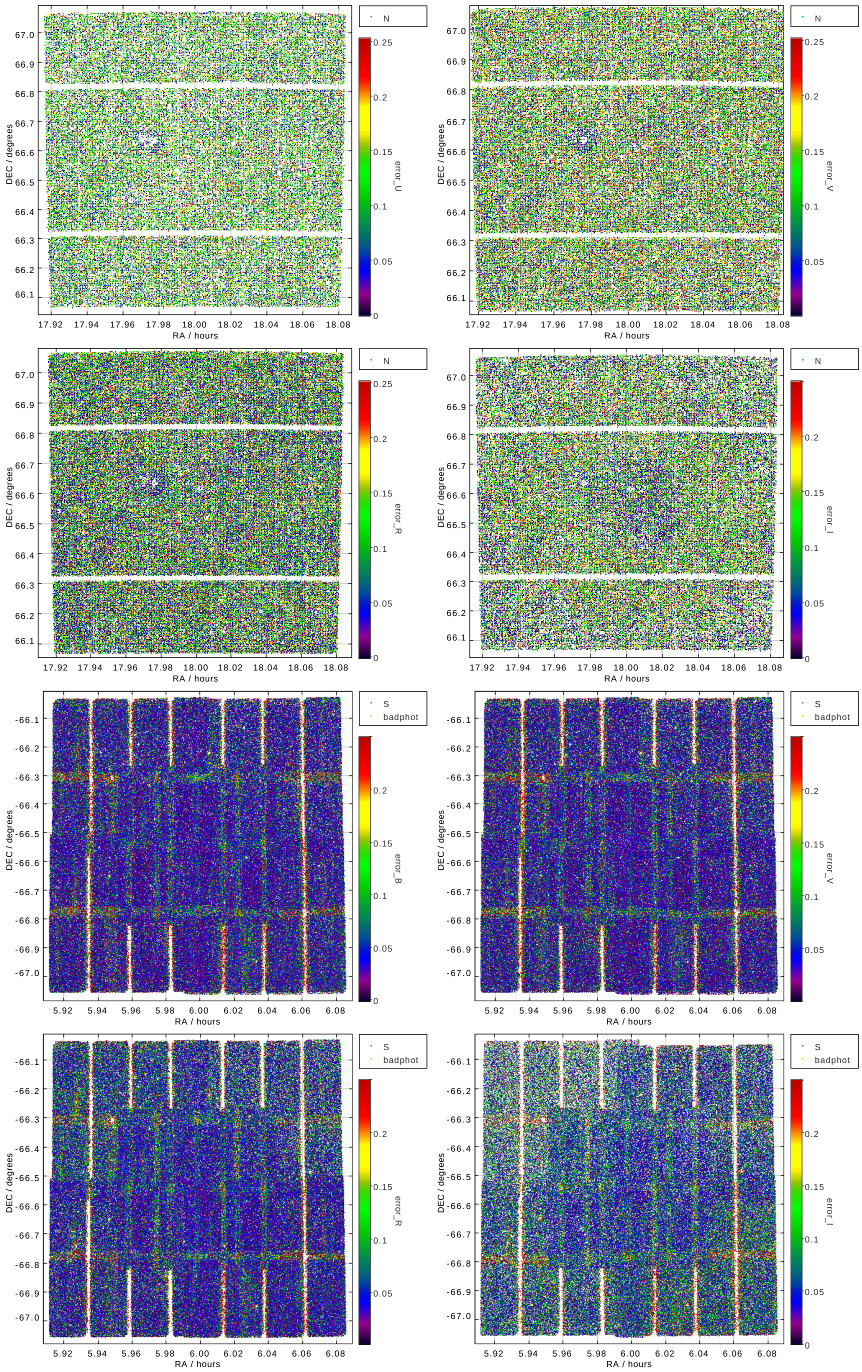

FIGURE 4: The spatial distribution of the r.m.s. errors of the GEPC photometry. The upper four panels show the situation for the northern field in the sequence u, g, r, i (upper left to lower right), the lower panels show the southern part in the sequence B, V, R, I (upper left to lower right). Please note that these plots represent the internal error only, external errors due to calibration, photometric system, etc. are not included. The SEP-field has more structure in its error distribution because of the 5 pointings approach, while the NEP was covered with one pointing (not to be confused with a dither pattern). Note the region near the gaps in the SEP-field where errors can be larger, caused by only a few stars being present in this regions and these being only covered by the short exposures. This is a consequence of the matching technique employed to minimise the number of false positives (see Sect. 2.5).

cision scale. Accuracy is now mainly limited by the underlying reference catalogue, which for the GEPC2/3 is the PPMXL (Roeser et al., 2010), while the earlier versions are based on the UCAC 2 catalogue (Zacharias et al., 2004). While the PPMXL is newer, the reference catalogue was not expected to have a large influence on the astrometry. However our experience shows that this is indeed the case. First of all, all available reference catalogues do have systematic differences, as is explained later in this text. Apparently not only the accuracy (i.e. systematic) effects, but also the precision plays a role and can lead to systematic effects in the reduced data. The reason for this is at current only partially understood, however most of the stars in the EPC field which are also in the reference catalogues, are in the faint part of the latter, consequently with a large error range, which will lead to ”sloppy” fits.

The registration and astrometric solution was done for each chip and each frame separately using the PPMXL as a reference and using 3rd order polynomials. An iterative method was used clipping 3-sigma outliers after the first round. The final positions were obtained using all of the good positional data, from all filters. This way we could ensure that every star has a valid position. We could not detect any sign of DCR. However since especially the U-band is prone to DCR, an alternative assembly of the final values might be considered in a future minor release.

For the NEP, we also excluded the long i-band images, since these produced large problems in the astrometry. For proper motions, we also added scans taken from the Minnesota Automated Plate Scanner (MAPS) Catalogue of POSS I[9] (see Pennington et al., 1993; Cabanela et al., 2003 of the relevant POSS I-plate (P72, taken 18. August 1952), in order to get a longer baseline, than the two years for which we have baselines. In order to also include high proper motions stars, we chose a large matching radius of 5”. In the current version we do not give errors for the proper motions, the according columns are thus completely nilled[10]. The scatter of the proper motions of the NEP field shows a sigma of about 10 mas/yr. This may well serve as an upper limit for the overall precision of the proper motions, since this value includes the proper motion and the positional error.

4.1 Errors

Concerning the astrometric precision, the error given for in the relevant columns for right ascension and declination reflect the r.m.s. error only, i.e. the scatter between the positions of all positions used to compile the position. The overall derivation of these errors is similar to those of the photometry, see Sect. 3.1 and equation 1. As in the case of most small field astrometry, we used a reference catalogue, which itself contains systematic errors to some degrees. These are not reflected in the errors as given in the EPC. One can presume zonal medium scale errors of about 50 - 100 mas. As an example, the PPMXL and 2MASS catalogues (which build up partially on the same data!) show a residual slope against each other of up to 50 mas. There-

[9]The MAPS database is supported by the University of Minnesota, available at `http://aps.umn.edu/`.
[10]this might be changed in future editions

fore the absolute astrometric positional accuracy cannot be better than this value. For proper motions, using the same reference catalogue for all epochs largely cancels out the systematic error introduced by the reference CATALOGS. For the NEP-field, which currently has proper motions, these show a sigma of about 10 mas/yr. This may well serve as an upper limit for the overall precision of the proper motions, since this value includes the proper motion and the positional error.

It should also be noted that neither the instruments used, i.e. mosaic detectors nor the available software are optimised for high precision astrometry, since they have largely been conceived and developed for extra galactic work, where the demands are much lower. Therefore some areas with additional systematics will exist, especially near chip edges, dither gaps etc. Even after the "final" release it will be attempted to minimise these as far as possible.

The astrometry of the southern part (GEPC2.1 incorporated into GEPC3.0) will be revised and completed for the next release (i.e. EPC4.0) with the addition of the second epoch data. We also intend to use old photographic plate (POSS) data to improve the proper motions.

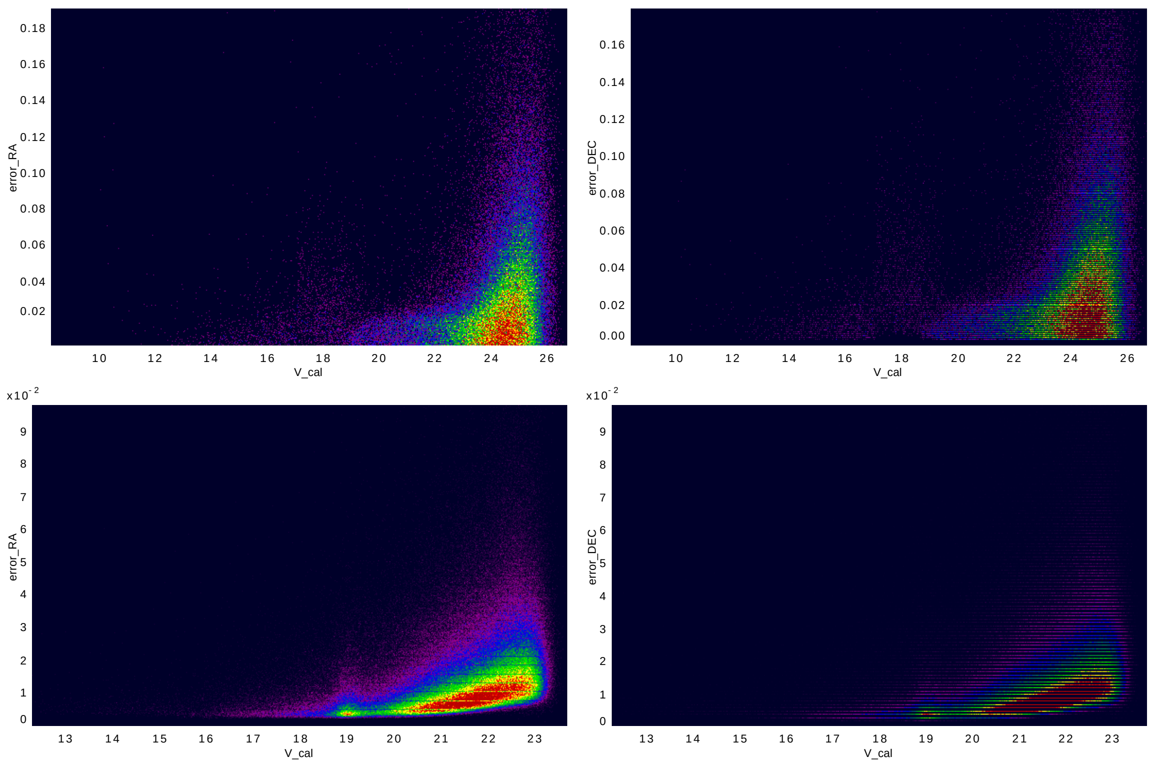

FIGURE 5: The r.m.s. errors of the GEPC astrometry in relation to the V,g magnitudes. The upper panels represent the northern field, the lower ones the southern. Left panels show R.A., the right ones Declination. Please note that these plots represent the internal error only, external errors due to calibration, reference catalogue, etc., which are substantially higher are not included.

5 Other quantities

5.1 Stellarity

Another quantity added to the GEPC is also the stellarity index also known as CLASS-parameter (Bertin & Arnouts, 1996). This is created during the source extraction from the 2d images using SExtractor. It is a measure for the ”stellarity” of an object, i.e. how star like it is. The stellarity index relies on a combined analysis of the measured morphological parameters, also employing neural networks. Values near 1 mean that it is very likely that this object is a point source like a star (it could of course also be the stellar nucleus of an AGN, etc., the stellarity index doesn’t say anything about the physical nature of an object). In reality one could consider all values below about 0.3 to be galaxies, i.e. non point source-like objects. S¿0.85 is a good lower limit for stars. At bright magnitudes, i.e. significantly above the detection limit, this classification works quite well, both object types are well separated, however about 2 mags above the detection limit it starts to break down, and soon the objects will not be classified correctly. This magnitude regime is also where most of the values between 0.3 and 0.85 occur. For saturated objects CLASS is also to be used with caution.

The northern field has a larger pixel scale than most other detectors, i.e. less angle per pixel. The neural networks on which the determination of the CLASS parameter of Sextractor is based are optimised for a FWHM of about 3 pixels. This means that the more the data deviates from this value, the less reliable the resulting CLASS value will be. This is not a linear process, but rather happens more or less suddenly - that it at least in this case already appears in the case of the NEP data is somewhat surprising. The networks can be trained for other FWHM values, however since this parameter was for the GEPC a secondary quantity, we did not embark on this tedious and difficult process.

5.2 Spectroscopically derived quantities, astrophysical parameters, radial velocities

This section will be filled in once the spectroscopic data is available and part of this documentation.

6 Format and Versions

6.1 Versions

6.1.1 EPC1.x

The first release of the GEPC (then still called EPC) 2009 was based on the first set of data, obtained in November 2007 with the 2.2 m MPIA telescope located at ESO's La Silla observatory and its WFI Mosaic type detector. Due to inclement weather conditions, no V-data was obtained, and R and I data only for 4 of the 5 proposed pointings - the SW-field was missing. Furthermore no useful calibration data was obtained, therefore the data for this release could only be roughly calibrated by tying the instrumental magnitudes to the literature values of the LMC red clump. The resulting calibration error is in the order of 0.3 mag. Nonetheless, this catalogue is still not obsolete, since it

- includes brighter stars than later versions, since saturated objects were not culled from the data - note that the values for their brightness get more and more unreliable with increasing brightness
- The object numbering is still used for the spectroscopy. A cross compilation catalogue (see Sect. 6.1.5 has been released which correlates EPC 1.x designations with those of later versions.

There are two subversion of this catalogue, the obsolete EPC1.0 and the valid EPC1.1, the difference between the two is, that the latter has all 4 G-type magnitudes, and the first version does not. A more detailed description of the EPC1.1, see MA-002[11].

6.1.2 GEPC2.x

The GEPC2.x catalogues have complete coverage of the southern field, i.e. including the SW-subfield. Additionally this version features the full and calibrated BVR_CI_C photometry of the southern field. The astrometry was changed in order to improve the previous results. While the precision is high, as is the internal accuracy, the overall accuracy has not been improved. This is presumably due to the quality of current reference catalogue material, which does not seem to be totally appropriate for high accuracy midsize field/mosaiced astrometry (see discussion elsewhere in this document). We are still striving to improve on this, currently independent meridian circle data are being taken for both fields. However any improved astrometry will only be available in later editions, after the commissioning phase. The object naming was changed in respect to the EPC1.x version, now it is a standard coordinate based nomenclature,

[11] the EPC1.0 is described in the obsolete document MA-001

i.e. **GEPCJ***HHMMSS.SS*σ*DDMMSS.S* (σ stands for sign). Saturated objects were culled from this version, therefore some bright stars, present in EPC1.1 are not included in GEPC2.1. The GEPC2.1 is - apart from a few formatting changes - the dataset for the south incorporated into the IGSL. The version history of this edition is as follows:

- GEPC2.0: **This version has a serious flaw in the right ascension coordinate, caused by a sign-error in the gnomonic projection. This means that at the central meridian of the catalogue, i.e. 06:00:00 the positions are correct, but away from this they are mirrored in respect to the central meridian line. For this reason the GEPC2.0 was retracted, and all copies deleted. Should any existing GEPC2.0 file be encountered, it should not be used and must be destroyed**
- GEPC2.1: This subversion replaces the former flawed version GEPC2.0 (see above). Since the data of GEPC2.1 is now incorporated into the current version 3.0, it could in principle be considered obsolete; However for reasons of convenience (i.e. having the more important southern field without the northern field), it can still be used.

Since the version 2.0 it was decided to call the catalogue GEPC, standing for **G**aia **E**cliptic **P**oles **C**atalogue, emphasising the use for the Gaia mission.

6.1.3 GEPC3.0

The current version adds the northern part and incorporates the previous GEPC2.1. Since this version is the main subject of this document, we refer to the description of the data in earlier sections.

6.1.4 Future Editions

- The next version will be GEPC4.0 which will include the U band data for the south and a bug fix of the $STELLARITY$ Parameter in the SEP-field (See Sect. 7). Taken from the IGSL, the bright stars will be added. Apart from this the NEP field data will stay unchanged.
- Version GEPC5.0 will contain spectroscopic data in the south, and possibly improved astrometry on one or both fields by adding meridional circle data.
- Version GEPC-NG (next Generation): This will a post first Gaia release edition with Gaia data used as reference catalogue material. This version will not be available before 2015.
- possible further versions may be considered after subsequent Gaia releases, creating a high precision Gaia calibrated astrometric field deeper than Gaia itself.

6.1.5 Special Versions

There are a few special purpose versions of the GEPC. Currently available is a catalogue cross referencing EPC1.1 and GEPC2.1/3.0, also including 2Mass NIR photometry for those stars bright enough to have this. However this catalogue is limited to objects, which are part of the GEPC2.1, i.e. some bright objects (which may be spectral targets), which are not in the GEPC2.1 are not in this list. In the immediate future it is planned to remedy this by repeating the cross match and including those stars.

More special purpose versions can be generated upon request.[12]

6.2 The Format of GEPC3.0

The current version of the catalogue is an ASCII file[13], other formats can be added on request (fits, votable, etc.). Since the catalogue was assembled using the TOPCAT (http://www.star.bristol.ac.uk/ mbt/topcat/)and STILTS (http://www.star.bristol.ac.uk/ mbt/stilts/) software packages, it complies with their conventions and can be readily read by either program.

Some of the photometry entries are empty; for those stars no value for that particular passband could be derived, either because the star was not covered by the data (pointings and thus field limits are a little different), or the particular star is too faint (or too bright) in this passband. Every star has at least one data from one passband, most have all four. Those fields which are empty have ”””” written in them. A large part of the work was done using VO-compatible software, such as topcat or stilts. This table will readily be read by either (when reading in this table with topcat, be sure to have chosen ’ASCII’ in the pull down menu which denotes the type of table to be read in; everything else, including ’auto’ will result in an error message). The running number identifier used in GEPC1.x has been replaced by an IAU conforming unique identifier based on an object’s position.

7 Caveats and known bugs

At current, there are 2 known bugs in this catalogue, both of rather minor importance, so that immediate action is not required. These will be further analysed and corrected once completely understood in the next release, i.e. GEPC4.0.

1. In the early stages of final assembly of the catalogue a switch in combination routine was set sub-optimally, leading to the suppression of objects which are only on two images or less on a set of 5 dithered images. This leads to the gap regions being only very sparsely populated. All

[12]Please contact Martin Altmann: `maltmann@ari.uni-heidelberg.de`
[13]this also applies to all other versions

TABLE 5: Fortran format of GEPC3.0: This table shows the formats and the columns in which the data is stored.

Name	Format	Unit	description
Obj_name	A23	—-	unique coordinate based identifier
RA_h	I2	hour	Right Ascension Hour
RA_m	I2	minute	Right Ascension Minute
RA_s	F7.4	second	Right Ascension Second
err_RA	F6.4	arcsec	Right Ascension Error
DEC_d	I3	degrees	Declination Degrees
DEC_m	I2	arcmin	Declination Minute
DEC_m	F6.3	arcsec	Declination Second
err_DEC	F5.3	arcsec	Declination Error
pm_RA	F8.2	mas/yr	proper motion in RA
err_pm_RA	F6.2	mas/yr	error of proper motion in RA, currently not used
pm_RA	F8.2	mas/yr	proper motion in DEC
err_pm_RA	F6.2	mas/yr	error of proper motion in DEC, currently not used
U_cal	F6.3	mag	calibrated U magnitude
err_U	F6.3	mag	error of U magnitude
B_cal	F6.3	mag	calibrated B magnitude
err_B	F6.3	mag	error of B magnitude
V_cal	F6.3	mag	calibrated V magnitude
err_V	F6.3	mag	error of V magnitude
R_cal	F6.3	mag	calibrated R magnitude
err_R	F6.3	mag	error of R magnitude
I_cal	F6.3	mag	calibrated I magnitude
err_I	F6.3	mag	error of I magnitude
z_cal	F6.3	mag	calibrated z magnitude
err_z	F6.3	mag	error of z magnitude
G	F6.3	mag	Gaia G magnitude
G_RVS	F6.3	mag	Gaia RVS magnitude
G_BP	F6.3	mag	Gaia BP magnitude
G_RP	F6.3	mag	Gaia RP magnitude
$Stellarity$	F4.2	—	Stellarity index, $\simeq 1 =$ star; $\simeq 0 =$ galaxy

TABLE 6: (Rough) star counts within 2 magnitude G-mag intervals for the complete catalogue, and the two fields. The last column gives the ratio between the number of stars in the SEP-field and those of the NEP-field, showing the increasing dominance at fainter magnitudes of LMC stars in the former field. Please note that the numbers in this table are not meant to be exact, since the intervals were determined by hand (the numbers for the North are the differences between the total and the south), and the areas of the fields are not exactly the same.

G-magnitude range	$\#stars$(All)	$\#stars$(NEP)	$\#stars$(SEP)	$\frac{\#stars(\text{SEP})}{\#stars\text{NEP})}$
12-14	446	208	238	1.14
14-16	2441	652	1789	2.74
16-18	9575	1531	8044	5.25
18-20	49450	2935	46515	15.85
20-22	212085	9039	203046	22.46

other objects are not affected. Meanwhile it has been attempted to rectify this problem, however with the consequence of a much larger number of false positive detections. Since false positives are detrimental for the Gaia commissioning process, this was not updated in any version 3.X. Please also note the following: i. even after the bug fix those regions of the field, which are touched by the chip gaps of the dither pattern, will have a lower start density and slightly lower precision of both photometry and astrometry. This is the nature of mosaic data and something that cannot be fixed. ii. For the NEP field a 36 chip mosaic was used. Here the 5 point dither pattern (the best compromise between observing time efficiency and exposure homogeneity), will lead to small gaps in the field, i.e. areas completely unexposed. Again this is unavoidable at reasonable costs.

2. For about 5% of the stars the parameter ”STELLARITY” is significantly higher than one, up to more than 100. This is presumably caused by a programming glitch in one of the assembly scripts (Initially stellarity was given as a number between 1 and 1000). The exact cause needs to be located. Again this problem is of minor nature and hence it will be fixed in the next incremental release 4.0.

Both of these bugs are restricted to the SEP-field and will be rectified in the next release.

8 The dataset

8.1 Star counts

While located at similar galactic latitudes and distances from the Galactic centre, the star count profiles of the two fields are very different, especially among the fainter stars. The reason for this is that the southern field is located in the Large Magellanic Cloud area, leading to a vast excess population of LMC stars. This can be seen, that while the SEP-field is more than 1 magnitude shallower than the northern field, it contains almost 3$\times$ as many stars (see Fig. 6). For stars brighter than $G \simeq$15 mag, both fields are comparable in star density[14], in the interval $G = [20, 22]$ mag the south contains more than 20$\times$ the number of stars as the north, see Table 6.

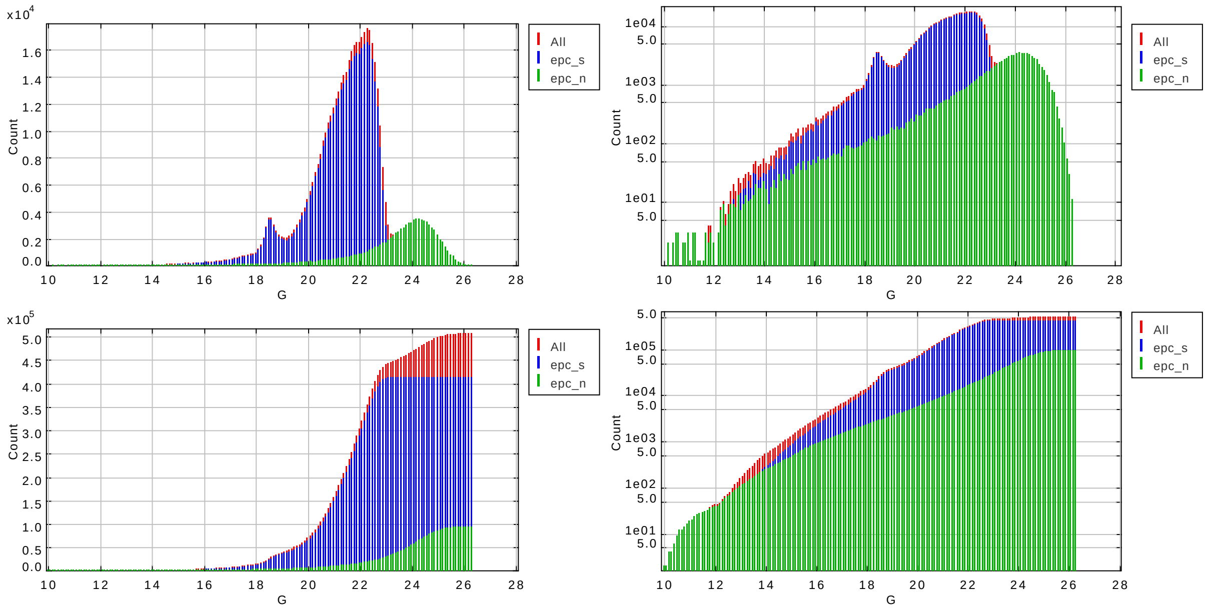

FIGURE 6: G-magnitudes histograms of the stars of the EPC (only those objects, for which we have G-magnitudes, i.e. both V and R resp. g and r magnitudes exist). Shown is always the total count in red, the SEP field's counts in blue and the NEP's counts in green. The upper panels show the normal (non-cumulative) histograms, the lower panels the cumulative histograms. The left panels show the linear plots, the right panels the logarithmic histograms.The "bump" only seen in the Southern field data, near G=18.5 mag is caused by the LMC red clump.

8.2 Colour-magnitude and colour-colour diagrams

[14] note that from about $G = 14$ mag on and brighter there is an increasing level of incompleteness, due to saturation of objects even on short exposures - this is different for each of the two fields

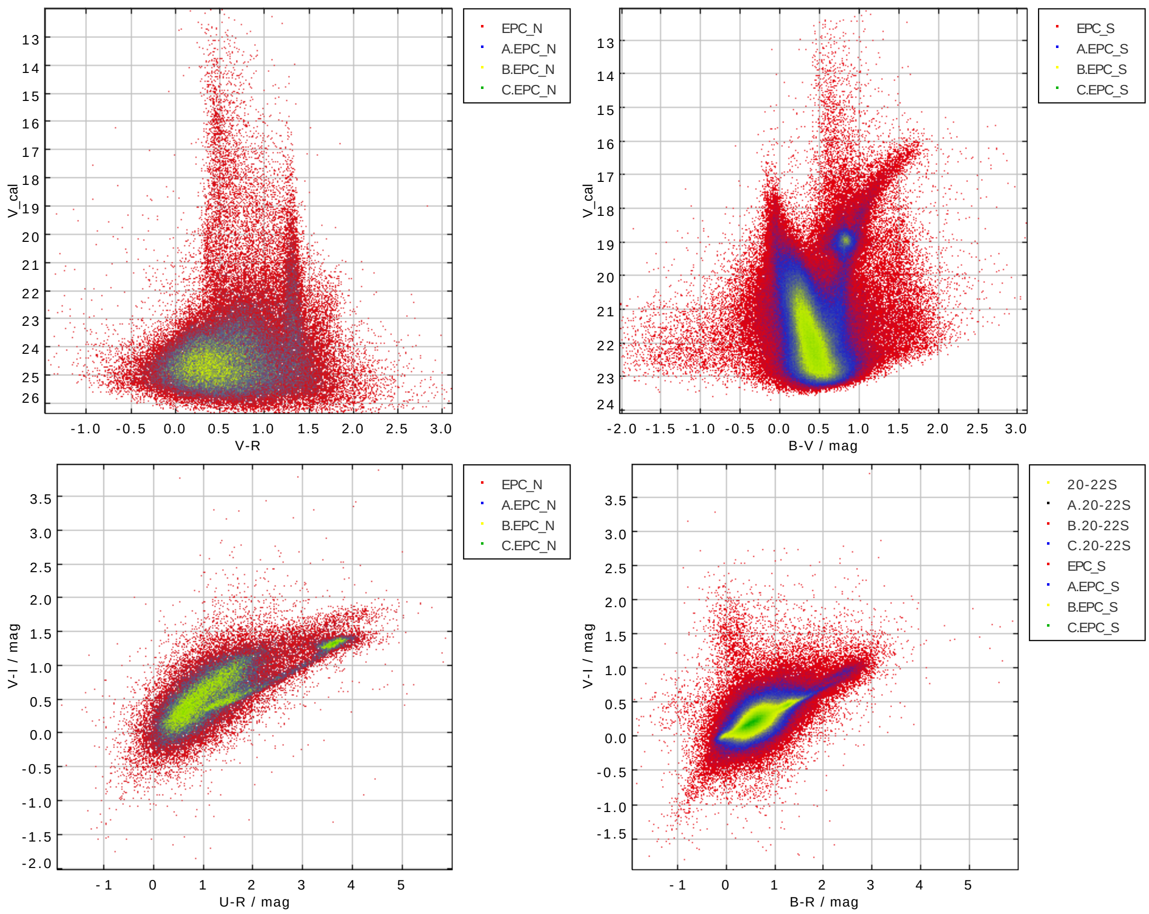

FIGURE 7: Colour-Magnitude (top) and Two-Colour-Diagrams of the two fields comprising the GEPC. The left hand side shows the northern field, and the right side the southern. Please note that the passbands used for each field are different (see Sect. 3

A Acknowledgements

This research has made use of the MAPS Catalogue of POSS I supported by the University of Minnesota. The APS databases can be accessed at `http://aps.umn.edu/`. Based on observations obtained with MegaPrime/MegaCam, a joint project of CFHT and CEA/DAPNIA, at the Canada-France-Hawaii Telescope (CFHT) which is operated by the National Research Council (NRC) of Canada, the Institut National des Science de l'Univers of the Centre National de la Recherche Scientifique (CNRS) of France, and the University of Hawaii.

B Additional Plots available in the Gaia SVN repository

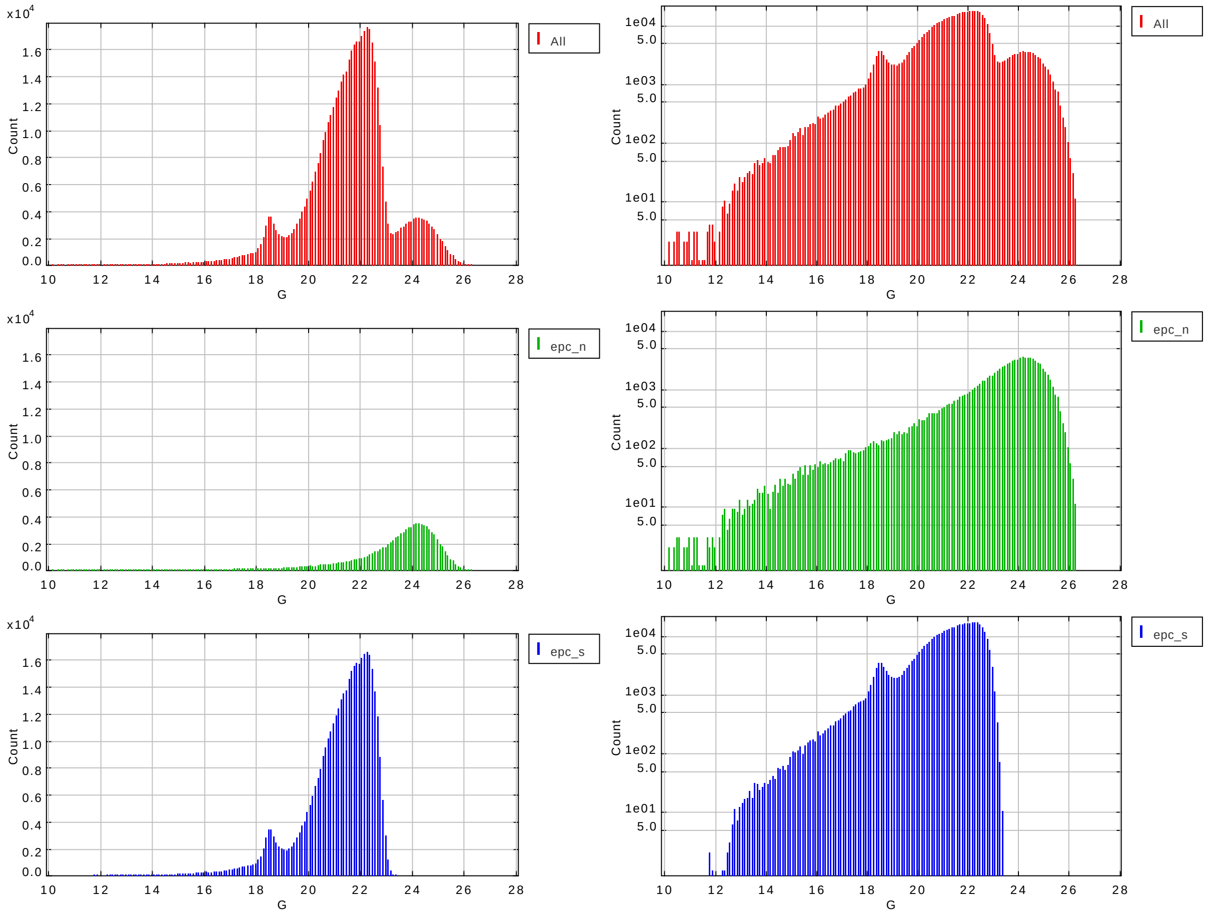

FIGURE 8: Additional G-magnitudes histograms of the stars of the EPC (See Fig. 6 for a description of the colours). The left panels show the linear histograms, the right ones the logarithmic ones. The upper row shows all stars, the middle ones the northern (NEP) field, and the bottom row the southern field

The plots in this appendix section are all available in the Gaia SVN repository under `http://gaia.esac.esa.int/dpacsvn/DPAC/CU3/docs/AuxDat/EclPol/EPC_PLOTS/` and are available the the use in presentations and Livelink documents. They are presented in this section to prevent to much clutter in the main section.

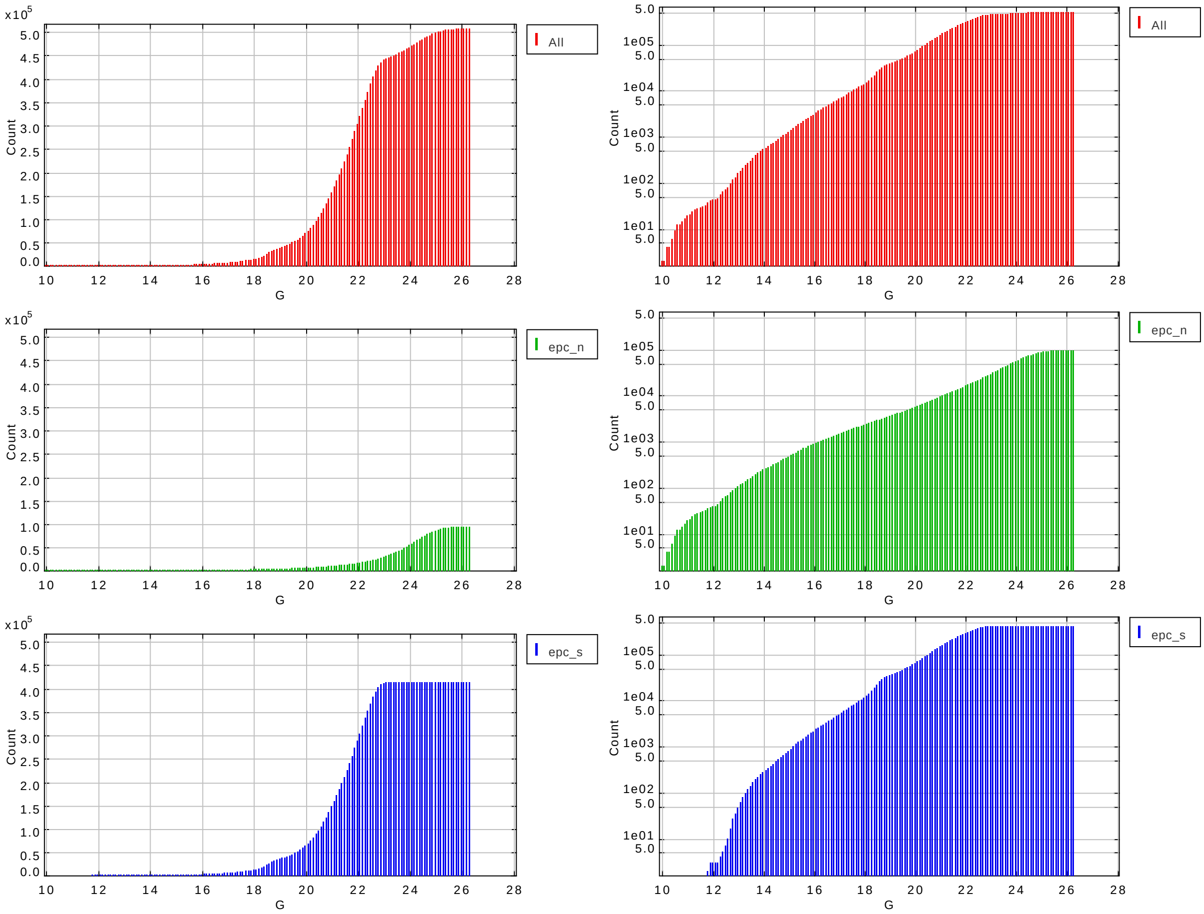

FIGURE 9: Additional G-magnitudes histograms of the stars of the EPC (See Fig. 6 for a description of the colours). The left panels show the linear histograms, the right ones the logarithmic ones. The upper row shows all stars, the middle ones the northern (NEP) field, and the bottom row the southern field

C Calibration equations and coefficients for the southern field

Calibration coefficients:

TABLE 7: The calibration coefficients, as derived with equations 2 to 8

Passband	Coeff. 1	Coeff. 2	Coeff. 3
B	$B1 = -0.9736133$	$B2 = 0.3664545$	$B3 = -0.2301114$
V	$V1 = -0.2362708$	$V2 = 0.2553625$	$V3 = +0.0842689$
R	$R1 = -0.4390256$	$R2 = 0.1548778$	$R3 = -0.0043028$
I	$I1 = +0.5818422$	$I2 = 0.1362779$	$I3 = +0.0127717$

Calibration equations:

$$(B-V)_{\rm cal} = \frac{(B-V)_{\rm inst} - (B1-V1) - B2\cdot AM_B + V2\cdot AM_V}{1+(B3-V3)} \tag{2}$$

$$B_{\rm cal} = B_{\rm inst} - B1 - B2\cdot AM_B - B3\cdot(B-V)_{\rm cal} \tag{3}$$

$$V_{\rm cal} = V_{\rm inst} - V1 - V2\cdot AM_V - V3\cdot(B-V)_{\rm cal} \tag{4}$$

$$(V-R)_{\rm cal} = \frac{(V-R)_{\rm inst} - (V1-R1) - V2\cdot AM_V + R2\cdot AM_R}{1-R3} \tag{5}$$

$$R_{\rm cal} = R_{\rm inst} - R1 - R2\cdot AM_R - R3\cdot(V-R)_{\rm cal} \tag{6}$$

$$(V-I)_{\rm cal} = \frac{(V-I)_{\rm inst} - (V1-I1) - V2\cdot AM_V + I2\cdot AM_I}{1-I3} \tag{7}$$

$$I_{\rm cal} = I_{\rm inst} - I1 - I2\cdot AM_I - I3\cdot(V-I)_{\rm cal} \tag{8}$$

The following numbers show the zero point shifting between the data and the calibration images, and the measurements of the latter with Sextractor and PHOT (from the daophot package). The according errors show the shift errors and are almost negligible.

Shift within calibration images between sextractor and PHOT (instr, $mag_{\rm sex} - mag_{\rm phot}$):

B:	-0.674	(σ=0.029,	Δ=0.0017),	275 stars
V:	-0.029	(σ=0.018,	Δ=0.0013),	179 stars
R:	-0.016	(σ=0.015,	Δ=0.0008),	331 stars
I:	$+0.226$	(σ=0.013,	Δ=0.0008),	276 stars

Shift between calibration images (sextr) and data zero level (instr $mag_{\mathrm{corr}} - mag_{\mathrm{sex}}$):

B: -0.050 (σ=0.016, Δ=0.0009), 299 stars
V: -0.038 (σ=0.017, Δ=0.0008), 476 stars
R: -0.148 (σ=0.032, Δ=0.0014), 481 stars
I: -0.136 (σ=0.019, Δ=0.0011), 279 stars

Total shift between data zero level and aperture photometry:

B: -0.724, (Δ=0.0019)
V: -0.067, (Δ=0.0015)
R: -0.164, (Δ=0.0016)
I: $+0.090$, (Δ=0.0014)

Since the calibration in the NEP field could be done on field using the data from Hwang et al. (2007) meaning only a magnitude shift was applied, we do not give the details here, since they are irrelevant.

D Formats of the older and special versions of the GEPC

D.1 Old Versions

TABLE 8: Fortran format of EPC1.0: This table shows the formats and the columns in which the data is stored.

Name	Format	Unit	description
$ObjNo$	I6	—-	unique numeric object identifier
RA_h	I2	hour	Right Ascension Hour
RA_m	I2	minute	Right Ascension Minute
RA_s	F7.4	second	Right Ascension Second
DEC_d	I3	degrees	Declination Degrees
DEC_m	I2	arcmin	Declination Minute
DEC_m	F6.3	arcsec	Declination Second
R_cal	F6.3	mag	R magnitude
I_cal	F6.3	mag	I magnitude

TABLE 9: Fortran format of EPC1.1: This table shows the formats and the columns in which the data is stored.

Name	Format	Unit	description
$ObjNo$	I6	—-	unique numeric object identifier
RA_h	I2	hour	Right Ascension Hour
RA_m	I2	minute	Right Ascension Minute
RA_s	F7.4	second	Right Ascension Second
DEC_d	I3	degrees	Declination Degrees
DEC_m	I2	arcmin	Declination Minute
DEC_m	F6.3	arcsec	Declination Second
R_cal	F6.3	mag	R magnitude
I_cal	F6.3	mag	I magnitude
G	F6.3	mag	Gaia G magnitude
Gf	I1	—	G magnitude flag
G_RVS	F6.3	mag	Gaia RVS magnitude
G_RVSf	I1	—	G magnitude flag
G_BP	F6.3	mag	Gaia BP magnitude
G_BPf	I1	—	G magnitude flag
G_RP	F6.3	mag	Gaia RP magnitude
G_RPf	I1	—	G magnitude flag

TABLE 10: Fortran format of GEPC2.x: This table shows the formats and the columns in which the data is stored.

Name	Format	Unit	description
Obj_name	A23	—-	unique coordinate based identifier
RA_h	I2	hour	Right Ascension Hour
RA_m	I2	minute	Right Ascension Minute
RA_s	F7.4	second	Right Ascension Second
err_RA	F6.4	arcsec	Right Ascension Error
DEC_d	I3	degrees	Declination Degrees
DEC_m	I2	arcmin	Declination Minute
DEC_m	F6.3	arcsec	Declination Second
err_DEC	F5.3	arcsec	Declination Error
B_cal	F6.3	mag	calibrated B magnitude
err_B	F6.3	mag	error of B magnitude
V_cal	F6.3	mag	calibrated V magnitude
err_V	F6.3	mag	error of V magnitude
R_cal	F6.3	mag	calibrated R magnitude
err_R	F6.3	mag	error of R magnitude
I_cal	F6.3	mag	calibrated I magnitude
err_I	F6.3	mag	error of I magnitude
G	F6.3	mag	Gaia G magnitude
G_RVS	F6.3	mag	Gaia RVS magnitude
G_BP	F6.3	mag	Gaia BP magnitude
G_RP	F6.3	mag	Gaia RP magnitude
$Stellarity$	F4.2	—	Stellarity index, $\simeq 1$ = star; $\simeq 0$ = galaxy

D.2 Special Versions

With special versions editions crossmatching identifiers from different GEPC-versions[15] and cross-matching with other catalogues are meant. Currently one version exists, matching the GEPC-IDs and the 2MASS catalogue (Skrutskie et al., 2006).

[15] currently two ID-versions are in existence, the EPC1 identifier which is a running number, and the position based GEPC2/3 identifier

TABLE 11: Fortran format of the first version of the GEPC3-EPC1-2MASS cross reference catalogue: This table shows the formats and the columns in which the data is stored. For more details about the 2MASS generic quantities and flags, please refer to the 2MASS publication article (Skrutskie et al., 2006)

Name	Format	Unit	description
Obj_name(GEPC2/3)	A23	—-	unique coordinate based identifier
$ObjNo$(EPC1)	I6	—-	unique numeric object identifier
RA_h	I2	hour	Right Ascension Hour
RA_m	I2	minute	Right Ascension Minute
RA_s	F7.4	second	Right Ascension Second
err_RA	F6.4	arcsec	Right Ascension Error
DEC_d	I3	degrees	Declination Degrees
DEC_m	I2	arcmin	Declination Minute
DEC_m	F6.3	arcsec	Declination Second
err_DEC	F5.3	arcsec	Declination Error
pm_RA	F8.2	mas/yr	proper motion in RA
err_pm_RA	F6.2	mas/yr	error of proper motion in RA, currently not used
pm_RA	F8.2	mas/yr	proper motion in DEC
err_pm_RA	F6.2	mas/yr	error of proper motion in DEC, currently not used
B_cal	F6.3	mag	calibrated B magnitude
err_B	F6.3	mag	error of B magnitude
V_cal	F6.3	mag	calibrated V magnitude
err_V	F6.3	mag	error of V magnitude
R_cal	F6.3	mag	calibrated R magnitude
err_R	F6.3	mag	error of R magnitude
I_cal	F6.3	mag	calibrated I magnitude
err_I	F6.3	mag	error of I magnitude
G	F6.3	mag	Gaia G magnitude
G_RVS	F6.3	mag	Gaia RVS magnitude
G_BP	F6.3	mag	Gaia BP magnitude
G_RP	F6.3	mag	Gaia RP magnitude
$Stellarity$	F4.2	—	Stellarity index, $\simeq 1$ = star; $\simeq 0$ = galaxy
$2MASSID$	A17	—	Identifier of object in the 2MASS catalogue
$Jmag$	F6.3	mag	J-magnitude in the 2MASS catalogue
e_Jmag	F6.3	mag	error of 2MASS J-magnitude
$Hmag$	F6.3	mag	H-magnitude in the 2MASS catalogue
e_Hmag	F6.3	mag	error of 2MASS H-magnitude
$Kmag$	F6.3	mag	K-magnitude in the 2MASS catalogue
e_Kmag	F6.3	mag	error of 2MASS K-magnitude
$Qflg$	A3	—	2MASS: JHK Quality flag
$Rflg$	A3	—	2MASS: JHK read (source) flag
$Bflg$	A3	—	2MASS: JHK Blend flag
$Cflg$	A3	—	2MASS: JHK contamination flag
$Xflg$	I1	—	2MASS: extended object flag
$Aflg$	I1	—	2MASS: association with known asteroid flag

E References

[MA-001], Altmann, M., Bastian, U., 2008, *Ecliptic Poles Catalogue Version 1.0*, `GAIA-C3-TN-ARI-MA-001`, URL `http://www.rssd.esa.int/llink/livelink/open/2863841`

[MA-002], Altmann, M., Bastian, U., 2009, *Ecliptic Poles Catalogue Version 1.1*, `GAIA-C3-TN-ARI-MA-002`, URL `http://www.rssd.esa.int/cs/livelink/open/2885828`

Bertin, E., Arnouts, S., 1996, A&AS, 117, 393, ADS Link

Bertin, E., Delorme, P., Bouy, H., 2012, *AstrOmatic Software in the Era of Large Stellar Photometric Surveys*, 71

Cabanela, J.E., Humphreys, R.M., Aldering, G., et al., 2003, PASP, 115, 837, ADS Link

Hwang, N., Lee, M.G., Lee, H.M., et al., 2007, ApJS, 172, 583, ADS Link

[CJ-041], Jordi, C., 2012, *Photometric relationships between Gaia photometry and existing photometric systems*, `GAIA-C5-TN-UB-CJ-041`, URL `http://www.rssd.esa.int/cs/livelink/open/2760608`

Magnier, E.A., Cuillandre, J.C., 2004, PASP, 116, 449, ADS Link

Pennington, R.L., Humphreys, R.M., Odewahn, S.C., Zumach, W., Thurmes, P.M., 1993, PASP, 105, 521, ADS Link

Roeser, S., Demleitner, M., Schilbach, E., 2010, AJ, 139, 2440, ADS Link

Schirmer, M., 2013, ApJS, 209, 21, ADS Link

Skrutskie, M.F., Cutri, R.M., Stiening, R., et al., 2006, The Astronomical Journal, 131, ADS Link

[RLS-004], Smart, R., 2013, *The Initial Gaia Source List and the Attitude Star Catalog*, `GAIA-C3-TN-OATO-RLS-004`, URL `http://www.rssd.esa.int/cs/livelink/open/3223578`

Taylor, M.B., 2005, In: Shopbell, P., Britton, M., Ebert, R. (eds.) Astronomical Data Analysis Software and Systems XIV, vol. 347 of Astronomical Society of the Pacific Conference Series, 29, ADS Link

[BV-001], Voss, B., Bastian, U., 2007, *The Ecliptic Poles Scanning Law and the Ecliptic Poles Catalogue*,
`GAIA-C3-SP-ARI-BV-001`,
URL `http://www.rssd.esa.int/cs/livelink/open/2737354`

Zacharias, N., Urban, S.E., Zacharias, M.I., et al., 2004, AJ, 127, 3043, ADS Link

F Acronyms

The following is a complete list of acronyms used in this document. The following table has been generated from the on-line Gaia acronym list:

Acronym	Description
AGIS	Astrometric Global Iterative Solution
AO	Announcement of Opportunity
AS	Adjacent Sample
ATP	Automatic Test Procedure
AUT	AUTomated
CCB	Configuration Control Board
CDR	Critical Design Review
CIL	Critical Items List
CM	Calibration Model
CNES	Centre National d'Etudes Spatiales (France)
CPU	Central Processing Unit
CSV	Comma-Separated Value (database output format, e.g., for MS Excel)
CU	Coordination Unit (in DPAC)
DDP	Delivered Duty Paid
DOC	Department of Commerce (USA)
DPAC	Data Processing and Analysis Consortium
DPC	Data Processing Centre
DPCE	Data Processing Centre ESAC
DU	Development Unit (in DPAC)
ECSS	European Cooperation for Space Standardisation
ESA	European Space Agency
ESAC	European Space Astronomy Centre (VilSpa)
FL	First Look
FLOP	FLoating-point OPeration
FTE	Full-Time Equivalent
GAIA	Global Astrometric Interferometer for Astrophysics (obsolete; now spelled as Gaia)
GWP	Gaia Work Package
HW	Hardware (also denoted H/W)
ICD	Interface Control Document
ID	Identifier (Identification)
IDT	Initial Data Treatment (Image Dissector Tube in Hipparcos scope)
ISO	International Organisation for Standardisation (Geneva, Switzerland)
JD	Julian Date

JDK	Java Development Kit
LaTeX	(Leslie) Lamport TeX (document markup language and document preparation system)
MAN	MANual
MDB	Main DataBase
OF	Object Feature (source packet)
PA	Product Assurance
PAP	Product Assurance Plan
PDR	Preliminary Design Review
PR	Progress Report
QA	Quality Assurance
RAM	Random Access Memory
SADT	Structured (System) Analysis and Design Technique
SCMP	Software Configuration Management Plan
SDD	Software Design Document
SDP	Supplementary Data Pattern
SP	SPecification
SPR	Software Problem Report
SRR	System Requirements Review
SRS	Software Requirements Specification
SSS	System Software Specification
STP	Software Test Plan
STR	Software Test Report
STS	Software Testing Specification
SUM	Software User Manual
SVN	SubVersioN
SW	Software
TRB	Test Review Board
TRR	Test Readiness Review
UML	Unified Modeling Language
URL	Uniform Resource Locator
WBS	Work Breakdown Structure
WP	Work Package